

Article

Metal Embedded Porous Carbon for Efficient CO₂ Cycloaddition under Mild Conditions

Chen Qi ^{1,*}, Somboon Chaemchuen ^{1,*}, Meng Liu ^{1,2}, Jichao Wang ^{1,2}, Serge Zhuiykov ³
and Francis Verpoort ^{1,4,*}

¹ State Key Laboratory of Advanced Technology for Materials Synthesis and Processing, Wuhan University of Technology, Wuhan 430070, China; chenqi1529368578@icloud.com (C.Q.); lmeng202201@163.com (M.L.); wangjichao_whut@163.com (J.W.)

² School of Materials Science and Engineering, Wuhan University of Technology, Wuhan 430070, China

³ Centre for Environmental & Energy Research, Faculty of Bioscience Engineering, Ghent University Global Campus, 119 Songdomunhwa-Ro, Incheon 21985, Korea; serge.zhuiykov@ghent.ac.kr

⁴ Research School of Chemistry & Applied Biomedical Sciences, National Research Tomsk Polytechnic University, Lenin Avenue 30, 634050 Tomsk, Russia

* Correspondence: sama_che@hotmail.com (S.C.); francis@whut.edu.cn (F.V.)

Abstract: Nitrogen-doped porous carbon material was generated via thermal pyrolysis of zeolitic imidazole frameworks (ZIFs). The structure of the ZIF templates was tuned, so that the obtained product was an N-doped porous carbon-containing encapsulated metal nanoparticle. The hierarchical structural and unique properties of pyrolyzed materials are involved in further application, including catalysis. The as-synthesized porous carbon materials were applied as a catalyst for CO₂ fixation on cyclic carbonates under near ambient pressure without solvent and co-catalyst. The zinc dispersion in highly porous carbon material, deriving from ZIF-8, exhibited a superior catalytic performance among the synthesized materials. The acid sites (Zn species) and the incorporated basic sites (N-species) present in the porous carbon material are essential for a high affinity for gas adsorption and CO₂ conversion. Additionally, the catalyst was found to be very robust and stable during recycling studies as the catalytic performance remained high for seven cycles.

Keywords: N-doped carbon; ZIFs; catalysis; pyrolysis; CO₂ utilization



Citation: Qi, C.; Chaemchuen, S.; Liu, M.; Wang, J.; Zhuiykov, S.; Verpoort, F. Metal Embedded Porous Carbon for Efficient CO₂ Cycloaddition under Mild Conditions. *Catalysts* **2022**, *12*, 427. <https://doi.org/10.3390/catal12040427>

Academic Editor: Leonarda Francesca Liotta

Received: 11 March 2022

Accepted: 4 April 2022

Published: 11 April 2022

Publisher's Note: MDPI stays neutral with regard to jurisdictional claims in published maps and institutional affiliations.



Copyright: © 2022 by the authors. Licensee MDPI, Basel, Switzerland. This article is an open access article distributed under the terms and conditions of the Creative Commons Attribution (CC BY) license (<https://creativecommons.org/licenses/by/4.0/>).

1. Introduction

Carbon materials have been widely investigated and have broad applications in academic research and industrial applications. Among all existing carbon-based materials, porous carbon has been viewed as the most important material due to its specific characteristics, including (i) excellent chemical, thermal and mechanical stability, (ii) tunable porosity and surface functional chemistry, (iii) good electrical and thermal conductivity, (iv) high surface area, (v) structural heterogeneity and morphology, and (vi) low cost and uncomplicated handling in the manufacture [1,2]. Due to those captivating properties, porous carbon is used in various applications as an adsorbent, catalyst, electrode relevant to energy conversion, and environmental chemistry [3–7]. Different routes are used to synthesize porous carbon material, including activation (physical or chemical), carbonization of polymer aerogels, synthetic template procedure, etc. [8–11]. Simple thermal pyrolysis of various organic precursors under a controlled atmosphere is a general process to obtain porous carbon material [12].

Nevertheless, the disordered and non-interconnected structures of thermally synthesized carbon greatly limit their application. Recently, metal-organic frameworks (MOFs) and zeolite imidazolate frameworks (ZIFs) have been evidenced to be ideal sacrificial precursors for synthesizing various carbon-based materials. Metal-organic frameworks

(MOFs) are among the most important and rapidly growing groups of porous materials. They are made of a combination of metal species and organic linkers. At the same time, zeolitic imidazole frameworks (ZIFs) represent one category of MOF materials comprised of imidazole linkers and metal ions (clusters), with a structure similar to zeolites. Due to various metal/organic linker species and the tunability of the frame, shape, and pore size, MOFs/ZIFs are very interesting and challenging [13–15]. Nevertheless, further development of suitable MOF materials for applications still requires improvement by several means, including chemical, physical, and thermal stability. Furthermore, the presence of the organic linkers in their framework possesses a high carbon content which can be seen as an excellent carbon source. Additionally, the metal ions/cluster and functional elements in the framework can transform the properties of carbon products during thermal decomposition (pyrolysis). A growing number of studies report the use of MOF/ZIF-template to synthesize porous carbon materials, especially in the energy and environmental areas, including batteries (e.g., lithium-ion, lithium-sulfur, and lithium-air batteries), supercapacitors, and gas adsorption and separation [16,17]. Although many studies on pyrolyzed MOF/ZIF-template have been reported in the past, few reports discuss their use in heterogeneous catalyses, such as oxidation, hydrogenation, dehydrogenation, bio-oil refining, and the Fischer–Tropsch process [18–20]. The metal/oxide nanoparticles doped porous carbon, derived from MOFs/ZIFs, could be advantageous for catalytic application in the heterogeneous phase. Using ZIF-67 as a template to derive cobalt in N-doped carbon (Co/CN) was reported as an efficient catalyst for organic transformations [21]. These hybrid materials exhibited excellent activity to convert nitroarenes under mild reaction conditions. However, the recyclability decreased in consecutive runs since the strongly adsorbed reaction species blocked the active sites. Concerning the CO₂ transformation, pyrolyzed ZnCo-ZIF with two metals embedded in a carbon matrix (Zn/Cn-ZIF-H₂/Ar-1000) was recently applied as a robust heterogeneous catalyst for the CO₂ addition into epoxide [22]. The bimetallic system (Zn/Co) containing Lewis acid sites (metal ions) and basic sites from the N-doped carbon matrix, was demonstrated to be an active catalyst for the CO₂ addition reaction. The easy magnetic separation of the catalyst from the reaction mixture was an extra benefit of this robust heterogeneous catalyst.

Herein, we report on the development of N-doped porous carbonaceous materials derived from green synthesized ZIFs (ZIF-8, ZIF-67, and ZnCo-ZIF). The porous carbon materials act as robust heterogeneous catalysts with excellent activities and selectivities for the CO₂ fixation reaction under free-solvent and co-catalyst conditions at near atmospheric pressure. Interestingly, the N-containing carbonaceous material exhibits excellent catalytic performance. Metals dispersion and the N-sites doped in the hierarchical porous carbon, originating from the ZIF-8 material, are essential in the mechanism for the CO₂ fixation reaction. Moderate reaction conditions are required using the synthesized porous carbon as a catalyst for the CO₂ cycloaddition into epoxides (optimized at 80 °C, 1bar CO₂ pressure, solvent-free, and no co-catalyst). The designed catalyst has several advantages, e.g., highly selective, robust activity, solvent-free, recyclable, and can lead to a new approach in heterogeneous catalyst development for CO₂ transformation. Moderate reaction conditions were obtained by optimizing the catalyst loading, temperature, and reaction time under near ambient pressure.

2. Results

2.1. Material Characterization

The ZIF materials (ZIF-8, ZIF-67, and Zn/Co-ZIF) were first synthesized and used as a template for N-doped porous carbon through the pyrolysis process. Using water as a solvent, a room temperature synthesis route was applied to synthesize the ZIFs template, since mild reaction conditions can be used in a green synthetic route. The synthesized ZIFs were characterized to confirm their characteristic properties, e.g., crystallinity, morphology, porosity, and thermal stability via X-ray diffraction (PXRD), SEM, BET, and TGA, respectively, as shown in Figures S2–S5. The characterization results revealed that the

synthesized ZIFs had similar characteristic properties as reported in the literature [23,24]. After that, the ZIF used as template materials was pyrolyzed under controlled conditions. The pyrolysis process destroyed the crystalline structure of ZIFs (1000 °C for 1 h at a flow rate of 50 cm³·min⁻¹ of 5% H₂ in Ar) as confirmed by X-ray diffraction analysis (Figure 1a). The broad peak at about 23°, observed in the pyrolyzed materials' diffraction pattern, was assigned to the carbon [002] diffraction. Next to the broad carbon peak, metallic crystal peaks were observed in the pyrolyzed material's diffraction pattern only for Co/CN and ZnCo/CN. In addition, the diffraction of metallic crystalline cobalt peaks (2θ of 44.3°, 51.5°, and 76.1°) was found to be more intense in Co/CN than ZnCo/CN, which can be related to the cobalt content of ZIF templates. Moreover, the metal sintering effect during the high pyrolysis temperature could also be a reason for the high diffraction intensity. On the contrary, a non-crystal diffraction pattern was observed for Zn/CN, which implied that the metal (Zn) is well-dispersed or that the sample is a metal-free porous carbon. As the pyrolysis temperature of Zn-ZIF is 1000 °C and zinc is known to evaporate at a temperature above 908 °C, there is a chance that the diffraction peaks of Zn may not be seen in the pyrolyzed sample [25,26]. The broad diffraction peak is assigned to amorphous carbon with a graphite-like carbon structure [27]. Furthermore, elemental analysis (ICP) was used to determine element content in the pyrolyzed material. The result revealed a tiny zinc amount in Zn/CN compared to the amount of zinc in the ZIF-8 template (Zn ≈ 28% wt.) (Table 1). A well-dispersed tiny zinc content could result in the absence of zinc crystal diffraction peaks in Zn/CN.

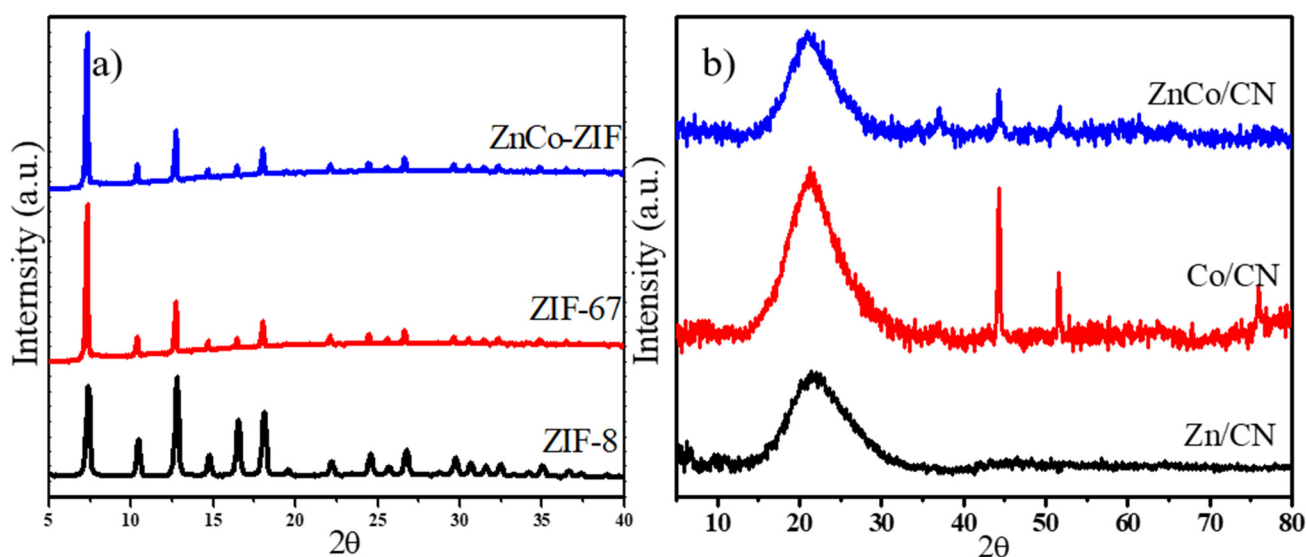


Figure 1. The pattern of XRD: (a) as-synthesized ZIFs, (b) pyrolyzed materials using different ZIF templates.

The morphologies of the materials were investigated using a scanning electron microscope (SEM). The rhombic dodecahedron shape with a particle size varying from 50–200 nm, depending on the type of ZIF template, was observed (Figure 2a–c). After pyrolyzing the template material, shape deformation and shrinkage were obtained. At the same time, numerous smaller nanoparticles (bright spots) were detected, demonstrating the presence of Co nanoparticles for ZnCo/CN and Co/CN, respectively, as depicted in Figure 2e–f. Additionally, it is worth mentioning that carbon nanotubes (CNTs) appear on the Co/CN, inset Figure 2f. Interestingly, the Zn/CN observes a slight surface shrinkage that keeps the rhombic shape similar to the ZIF-8 template. More in-depth morphological analyses applying transmission electron microscopy (TEM) were performed, and shape deformation and shrinkage phenomena were observed in the pyrolyzed samples, namely, Zn/CN and Co/CN obtained from the ZIF-8 and ZIF-67 templates, respectively (Figure 3). For the

Zn/CN sample, no metallic zinc nanoparticles were observed, confirming the observation made by XRD (Figure 1b,c).

Table 1. The porosity properties, CO₂ adsorption and C, N element analysis of porous carbon materials deriving from ZIF templates.

Porous Carbon/ZIF Template ¹	Surface Area (m ² ·g ⁻¹)			CO ₂ Adsorption (cm ³ ·g ⁻¹) ³	Elemental Analysis (% wt.) ⁴			
	BET	Langmuir	External ²		Zn	Co	N	C
ZIF-67	664	714	196	21	0.00	27.84	25.15	43.08
ZnCo-ZIF	694	747	227	21	16.02	16.43	24.48	41.85
ZIF-8	646	696	238	20	27.74	0.00	24.24	43.08
Co/CN	151	164	158	8	0.00	28	6.89	27.63
ZnCo/CN	205	221	185	12	0.05	5.85	1.90	53.73
Zn/CN	1525	1650	707	104	1.80	0.00	3.45	61.99

¹ All materials were pyrolyzed for 1 h under a 50 cm³·min⁻¹ flow of 5% H₂ in Ar. ² External surface area (t-plot) is the total surface area of materials, excluding the micropore surface area. ³ Adsorption at 273 K and CO₂ partial pressure up to 101 kPa. ⁴ C, H, O, N elements were determined by elemental analysis.

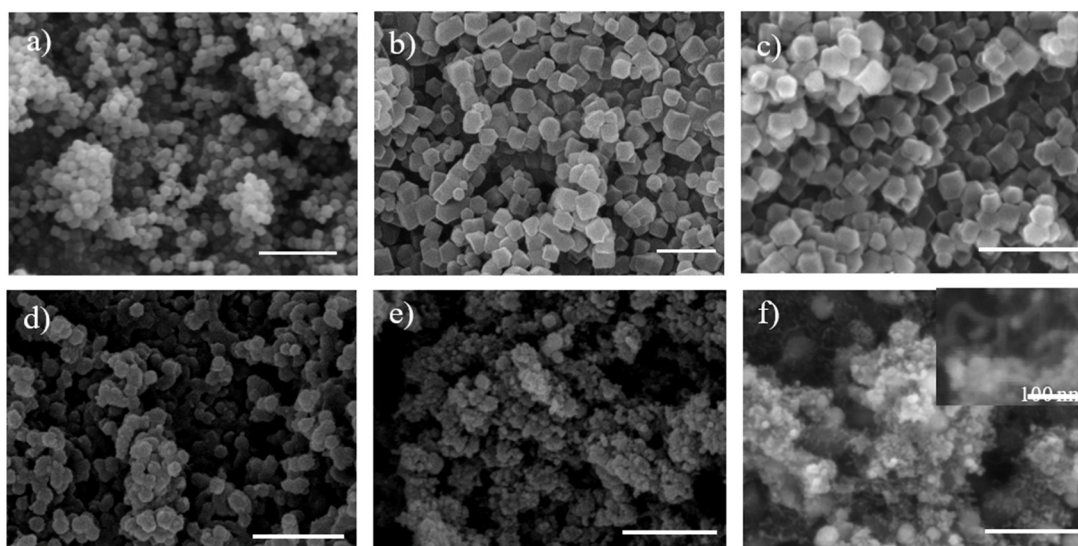


Figure 2. The morphology of the ZIF templates as-synthesized: (a) ZIF-8, (b) ZnCo-ZIF, (c) ZIF-67 and after pyrolysis: (d) Zn/CN, (e) ZnCo/CN, (f) Co/CN. The scale bar is 500 nm.

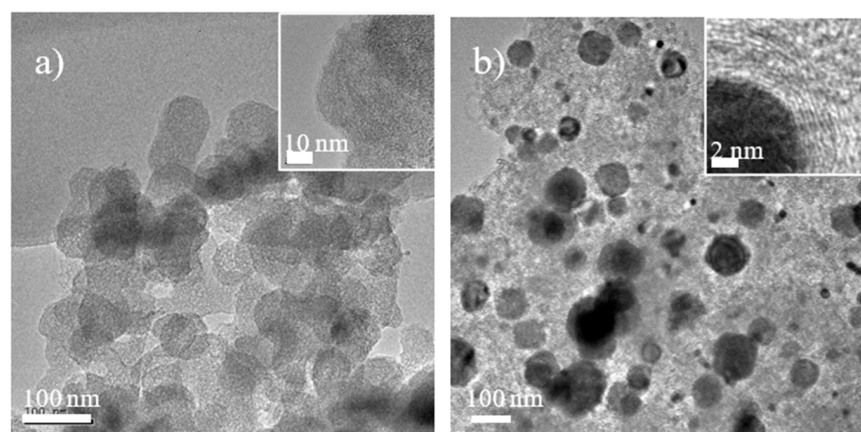


Figure 3. Transmission electron microscopy (TEM) image of porous carbon Zn/CN (a), and carbon layer in Zn/CN (inset in (a)), Co/CN (b) and carbon matrix layered coating on cobalt in Co/CN (inset in (b)).

Interestingly, the TEM image of Zn/CN, Figure 3b, exhibits a uniform layered carbon matrix generated during the pyrolysis of ZIF-8. Moreover, the absence of zinc-based nanoparticles or clusters in the TEM image of Zn/CN suggests that Zn atoms could exist in an atomic dispersion or were eliminated during pyrolysis. While for Co/CN, metallic Co nanoparticles in various particle sizes (10–100 nm) were observed (Figure 3b). The TEM image demonstrates that the Co nanoparticles are embedded in layers of carbon (Figure 3b, inset picture), thus stabilizing the cobalt nanoparticles.

ZIFs are intrinsically porous materials, and their pyrolysis inevitably causes the escape of volatile compounds and metals, producing different levels of porosities. The porosity properties of pyrolyzed materials were analyzed by N₂ physisorption analysis. The adsorption below the relative pressure (P/P_0) < 0.05 significantly decreases for the Co/CN and ZnCo/CN compared to their templates (Figures 4 and S6). These results indicate a diminished micropore content of pyrolyzed materials. Consequently, the surface area of those pyrolyzed products is significantly reduced compared to their pristine templates (Table 1). On the contrary, the N₂ isotherm at a low relative pressure (P/P_0 < 0.05) increases significantly for Zn/CN (>two times) compared to the ZIF-8 template. The template structure decomposes, and the organic linker (2-Methyl-Imidazole; 2-MIM) in the template framework gets transformed into carbon material during the pyrolysis process. Simultaneously, zinc elimination from the framework occurs, maintaining the pore structure, and causing high adsorption of N₂ on Zn/CN. The specific surface area values increased in the order Co/CN < ZnCo/CN < Zn/CN (Table 1, and Figure S6). Therefore, the N₂ isotherms are of *type IV* for the pyrolyzed materials, while the small hysteresis at the medium relative pressure ($0.45 < P/P_0 < 1.0$) suggests the presence of mesopores. These isotherms confirm the pyrolyzed materials' hierarchical porosity (mixed micro-mesoporosity). The material characteristics regarding the pores, spanning from the micro to the larger pores (meso or macropore), are consistent with reports on pyrolyzed MOFs or ZIFs [28]. Consequently, as given in Table 1, pyrolyzed ZIF-8 (Zn/CN) exhibited the highest surface area (1525 m²·g⁻¹) followed by ZnCo/CN (205 m²·g⁻¹), and Co/CN (151 m²·g⁻¹), respectively. Additionally, a difference in mesopore size distribution was observed in the order of Zn/CN > ZnCo/CN > Co/CN, respectively (Figure S6), which could be attributed to the metal (Zn) elimination during the pyrolysis process. Moreover, the metal elimination during the pyrolysis process could enlarge the porosity compared to the metal embedded pyrolyzed product. The enhanced pore size (micro to mesopore) might probably be due to the metal ions/cluster mobility (e.g., agglomeration, sintering) and generating additional pores during the framework decomposition at the high temperature of the pyrolysis process. However, the high thermal stability of cobalt resulted in the metal agglomeration into crystalline nanoparticles and the embedment in carbon materials and blocking of micropores, reducing the pyrolyzed product's total pore and surface area.

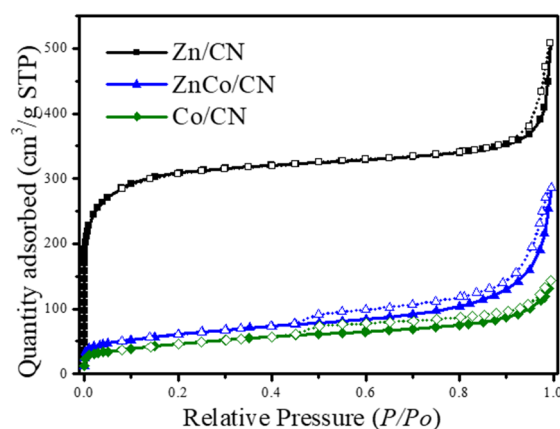


Figure 4. The N₂ isotherms of synthesized porous carbon materials deriving from ZIF templates.

The elemental analysis revealed that Zn/CN has the highest C percentage over ZnCo/CN and Co/CN (Tables 1 and S2). With the increasing pyrolysis temperature, zinc was eliminated from ZIF-8 and, to a lesser extent, from ZnCo-ZIF. Cobalt remained in ZnCo/CN and Co/CN after pyrolysis due to the higher evaporation temperature of cobalt. These effects could originate from the presence of different elements in the template materials. Nevertheless, pyrolysis reduced the N percentage in the samples compared to the percentage in their template. Co/CN has the highest N percentage, followed by ZnCo/CN and Zn/CN, respectively. The frameworks' thermal stability from high to low stability is given by: ZIF-67 > ZIF-8 > ZnCo-ZIF (TGA, Figure S4). These results imply that the strong M–N interaction enhances the N-content in pyrolyzed materials. The surface functional groups on pyrolyzed materials can differ according to the ZIF template's chemical environment, resulting in different chemical properties [29]. FT-IR analysis was performed on the pyrolyzed materials to gain information regarding their chemical bonding and surface functional groups. The FT-IR spectra reveal that the original M–N stretch modes (M: Zn or Co) at 421 cm^{-1} disappears in the pyrolyzed materials (Figure S7). This result confirms that the framework in ZIF templates was destroyed during the pyrolysis process. However, peaks at 1608 and 1250 cm^{-1} , derivative stretching and bending mode of N–H, and C–N, respectively, confirm chemical bonding between carbon and nitrogen in the pyrolyzed materials [30]. Interestingly, all pyrolyzed materials typically exhibit a band at 3423 cm^{-1} , assigned to the N–H and/or O–H symmetric stretching vibration [31,32]. Furthermore, the band characteristic of the presence of an aromatic ring peak at 1608 cm^{-1} for the carbon material (C=C stretching vibration) is observed in the pyrolyzed materials.

XPS analysis of the pyrolyzed samples was performed to investigate the elemental composition and chemical states of various elements. The survey analyses revealed Zn, Co, C, O, and N in the samples, as shown in Figure 5a. The high-resolution N 1s spectra were deconvoluted into three peaks with centers at 397.5, 400.5, 401.6 eV, describing the contribution of coordinated quaternary pyridinic-N, pyrrolic-N, and ammonium-N, respectively (Figure 5b). Different ZIF templates exhibited a variation in the ratio of N-species under the same pyrolysis conditions. The deconvolution of N-spectra reveals an increasing proportion of pyrrolic N species according to Co/CN < ZnCo/CN < Zn/CN. The opposite trend is observed for the ammonium-N species according to Co/CN > ZnCo/CN > Zn/CN. Notable, pyrrolic N species were reported earlier in the literature, having an excellent effect on the catalytic activity for the CO₂ cycloaddition with epoxides [22,33]. These pyrrolic N species, obtained from pyrolysis of ZIFs, serve as base sites, the active sites in the catalytic reaction (more discussion was provided under the section reaction mechanism). The Zn 2p high-resolution spectra display two peaks at 1021.1 eV and 1044.2 eV, assigned to Zn 2p_{3/2} and Zn 2p_{1/2} in Zn/CN and ZnCo/CN (Figure S8). Zn/CN revealed an excellent catalytic activity among the N-doped porous carbon samples compared with ZnCo/CN and Co/CN.

During pyrolysis, the ZIFs materials were heated at high temperatures under a controlled gas atmosphere. 2-methylimidazole, used to construct the ZIF material, served as the primary source of carbon formation with nitrogen content (CN). The characteristic materials indicate that pyrolysis conditions generated a different type of metal in N-doped porous carbon, which could involve the formation of active sites. Moreover, N-species are doped in the carbon, resulting in functionalized/doped carbon matrices creating unique properties of the generated carbon materials. The influence of different pyrolysis conditions on ZIF material (Zn/Co-ZIF synthesized via the spray drying method) was investigated in a previous report [22]. Metal oxide was generated in the presence of oxygen (air) during the thermal process. In comparison, during the pyrolysis process under an inert atmosphere, the metal ions/clusters became mobile and formed nanoparticles embedded in the carbon matrix derived from the organic ligand decomposition. Moreover, under a reduced atmosphere such as H₂/Ar mixture atmosphere, metallic species were obtained, which exhibited the best catalytic performance for the CO₂ cycloaddition with epoxides into cyclic carbonates [28].

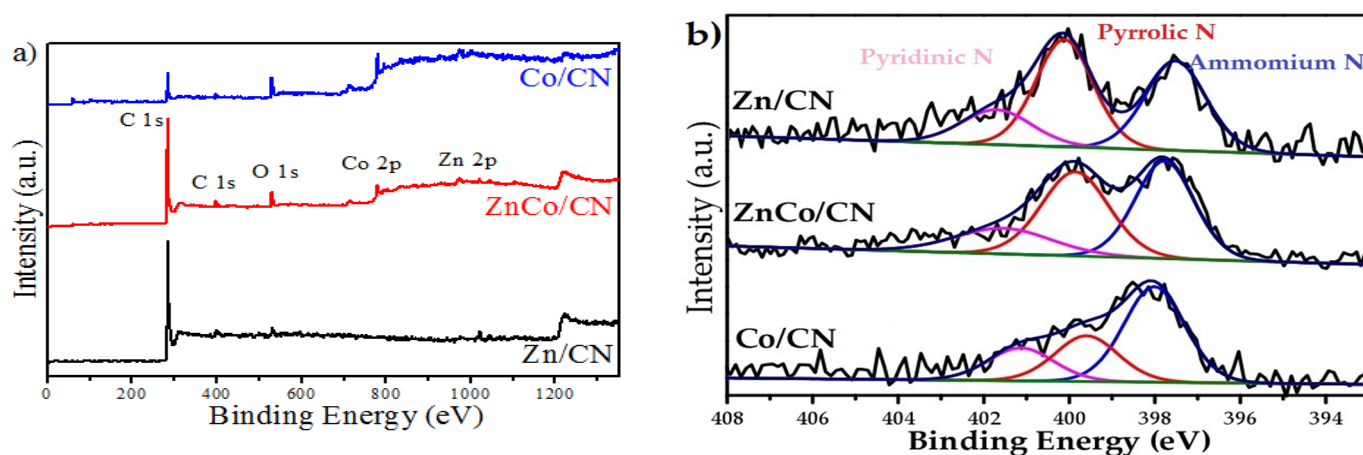


Figure 5. XPS survey analysis of carbonized materials (a), High-resolution N 1s spectra of species from different ZIF templates (b).

2.2. Catalytic Activity

Due to the regular arrangement of elemental species in ZIF precursors, the carbon composites contain nanostructured species prone to be formed during the in situ pyrolysis process. Furthermore, the N present in the imidazole linker could effectively functionalize the carbon structure. These facile synthetic approaches provide a new way to prepare porous carbon. Carbon materials derived from ZIFs have been widely explored for electrochemical energy storage applications with specific surface areas and capacitance performances [34–36]. The pyrolyzed materials demonstrate excellent chemical and thermal resistance, which are clear advantages over the template materials (ZIFs). Thus, promising applications not possible with common MOFs (ZIFs) materials are now within reach. Inspired by those reasons, the functional carbon materials were applied as heterogeneous catalysts for CO₂ fixation. Furthermore, milder reaction conditions (near ambient pressure) were used to pursue a “green reaction” without solvents and a co-catalyst. A “green reaction” would reduce byproducts, pollution, and risks to human health. Consequently, a highly selective heterogeneous catalyst was made without the need for downstream processes. The catalyst also exhibited excellent recyclability behavior in catalytic performance and stability, confirming that a truly heterogeneous catalytic system was created.

2.2.1. Catalytic Studies

In this study, the porous carbon materials derived from ZIFs were applied as a catalyst for the CO₂ cycloaddition into epoxides to produce cyclic carbonates. The catalytic performance of the various N-doped porous carbon products was assessed using epichlorohydrin as a model substrate, as shown in Figure 6. The synthesized carbon materials exhibited a significantly different catalytic activity under the same reaction conditions. The Zn/CN revealed the highest catalytic performance among comparative catalysts. Whereas no activity was observed using reference carbon as a catalyst, similar to the blank reaction (without catalyst). These results show the significance of the catalyst in the model reaction. To illustrate the special properties of the synthesized N-doped porous carbon, commercial carbon and starting precursors were investigated (Table S3, entries 9–15). It must be mentioned that ZIF templates, when used as catalysts, achieved excellent catalytic performance (Table S3, entries 3–8); however, the decomposition, metal leaching, and organic ligand contamination in the product are severe drawbacks of those catalysts. Meanwhile, the metal species (ZIF-8, ZIF-67, ZnCo-ZIF, ZnO, ZnCO₃, pyrolyzed Zn(NO₃)₂·6H₂O, Co(NO₃)₂·6H₂O), and pyrolyzed Co(NO₃)₂·6H₂O, which might be present in pyrolyzed materials from the ZIF templates, were also applied as a catalyst in the model reaction. No or a minimal yield of cyclic carbonate (6% yield with ZnO) was obtained, see Table S3. The catalytic activity of

commercial carbon materials was also studied. Nevertheless, no product was obtained with carbon, while a small product yield (5%) was acquired with carbon graphite oxide as a catalyst in a similar condition (Table S3). Nevertheless, impurities deriving from the synthesis of commercial carbon graphite oxide (such as iron) and the CO₂ adsorption ability of graphite oxide might provide some catalytic activity as well [37,38]. Remarkably, the 2-methylimidazole (2-MIM), the linker in the ZIF structure, performed excellently (100% Conv., 90% Yield). This result evidenced that the basic sites of 2-MIM can activate CO₂ (see discussion of the mechanism). However, it is impossible to recycle 2-MIM as a catalyst from the reaction mixture, which is the main drawback of applying 2-MIM as a catalyst. An alternative is the removal of the obtained cyclic carbonate by distillation, after which the remaining 2-MIM can be reused. However, the latter procedure is energy demanding. Therefore, all results reveal that the pyrolyzed carbon materials derived from ZIFs, especially Zn/CN, show excellent catalytic activities.

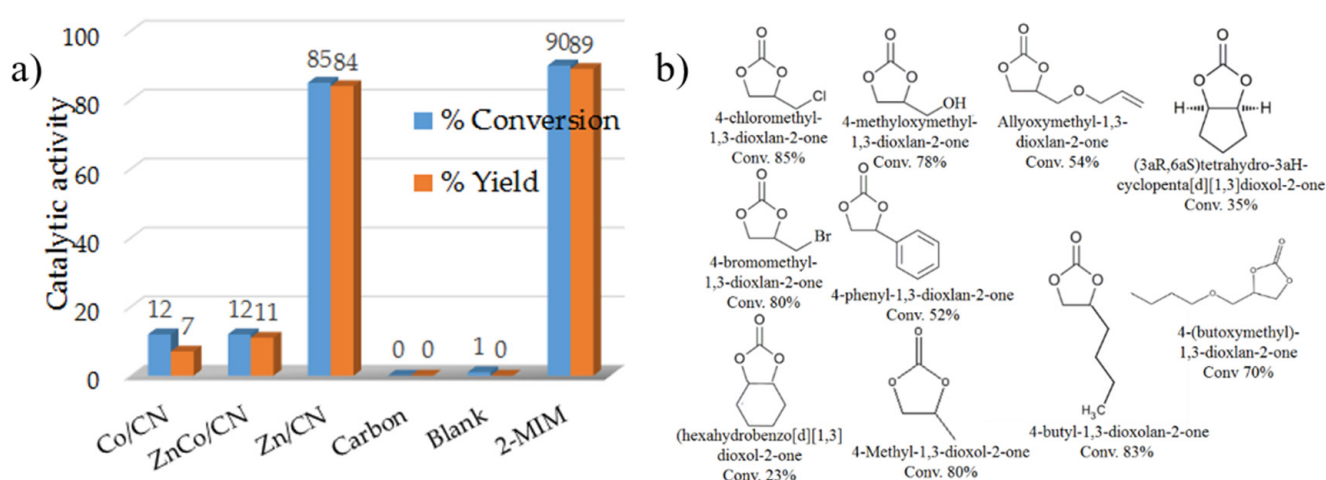


Figure 6. (a) Catalytic performance of synthesized porous carbon materials obtained from different ZIFs and pyrolysis temperature. (b) Variety of cyclic carbonates produced by Zn/CN as catalyst. Conversion and yields were determined by ¹H NMR and using 1,3,5-trimethylbenzene as the internal standard. The details of experiments are provided in Table S3.

Particularly for commercial applications, the heterogeneous catalyst shows an essential advantage over the homogeneous catalysts, namely for catalyst separation and recovery. Another major concern of the catalyst is its stability. The reusability of the catalyst was investigated by using Zn/CN. The spent catalyst was separated from the reaction mixture via centrifugal and washed with methanol five times before drying in a vacuum oven at 100 °C overnight. The weight of the recovered catalyst was measured before reuse for each subsequent experiment (run 2–7). The perceived results indicate that each cycle's catalytic activity remains excellent (conversion and product yield), as shown in Figure 7.

Moreover, the catalyst weight was maintained after each recovery. The characteristic properties of the catalyst after reaction were determined, such as XRD, XPS, N₂ adsorption, porosity, and surface area analysis. The characteristic results were similar to the fresh catalyst (Figures S10 and S11). These results evidence that Zn/CN is a robust catalyst that can be reused without losing catalyst weight and catalytic performance. Nevertheless, the conversion decreased slightly using a double amount of ECH moles under similar reaction conditions using Zn/CN (Table S3, entries 13, 17).

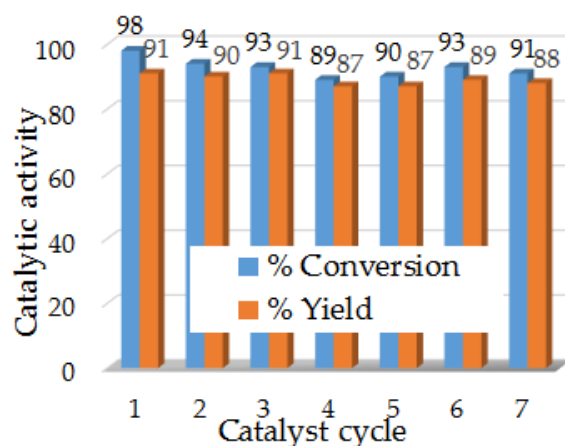


Figure 7. The recyclable catalyst using 9.2 mmol ECH, catalyst Zn/CN (50 mg) at 90 °C, 1 bar CO₂ pressure for 24 h. Conversion and yields (isolated) were determined by ¹H NMR and using 1,3,5-trimethylbenzene as the internal standard.

The catalytic performance of the applied carbon materials with the reaction conditions and catalytic outcome are summarized in Table S4. Next, the performance of Zn/CN was investigated for different epoxides, and excellent conversions were obtained (Figure 6b, Table S3, entries 16–25). The substrates containing electron-withdrawing substituents exhibit a higher conversion via an enhanced easiness of the ring-opening of the epoxide, allowing the nucleophilic attack followed by carbonate formation. The results confirm that a high selectivity is obtained using Zn/CN as a catalyst. Nonetheless, it needs to be mentioned that the formation of some amounts of oligomeric or polymeric carbonates in the case of certain epoxides cannot be excluded, as was evidenced by some broad peaks in the ¹H NMR spectra (see Figures S14–S18). However, a reduced yield (less than stoichiometric yield) is mainly associated with strong chemisorption of cyclic carbonates by the oxygen functionalities present on the pyrolyzed catalyst surface, or adsorption in the pores of the catalyst (high micro/mesopore porosity). Several catalytic systems have been reported for cycloaddition of CO₂ into epoxides, including carbon-based materials.

2.2.2. Reaction Mechanism

Several studies in the literature report that acid sites originate from transition metals, while the basic sites derive from the N-species in the carbon catalyst made from MOFs/ZIFs. Both acid and basic sites are the active sites for the CO₂ cycloaddition [22,39]. Moreover, it is well known that an organic base can activate CO₂, and this activated species, in its turn, acts as a Lewis base to open the epoxide ring [40–42]. The catalytic mechanism describing the basic sites as the activating species for epoxides in the cycloaddition with CO₂ to cyclic carbonates was recently reported for the N-doped carbon catalyst (carbon material) [42,43]. Herein, the catalytic performance of Zn/CN demonstrated the highest catalytic activity among the pyrolyzed catalysts (Co/CN and ZnCo/CN). To gain insight into the basic properties of the catalytic material, chemisorption analysis (CO₂-TPD) was performed, and the obtained profiles are depicted in Figure S9. The CO₂ desorption profile revealed that the adsorbed CO₂ mainly desorbs between 510 °C and 684 °C, confirming the strong basic properties of the synthesized materials. Interestingly, the CO₂-TPD profile obtained from Zn/CN reveals that a significant part of the adsorbed CO₂ is desorbed at a lower temperature (510 °C) compared to ZnCo/CN (684 °C). In contrast, the smallest amount of desorption was observed in the profile obtained from Co/CN. The basic properties, generated from the N-species of the linker (2-MIM), could be enhanced by the metal elimination during the pyrolysis process [44]. Although the calculated distributions of the different N-types were obtained via XPS analysis, it is clear that Zn/CN possesses the highest amount of pyrrolic N (Figure 5b). This characteristic property (basicity) is significantly related to the increasing catalytic performance.

Moreover, the different starting compounds to construct the catalytic material were investigated, and complete conversion was observed using only the linker (2-MIM) as a catalyst (Table S3, entries 3–15). This high conversion is attributed to the basic sites present in 2-MIM. The catalytic reaction occurs at basic sites (N-doped porous carbon) together with the metals (acid sites, e.g., Co or Zn) as active centers. It is also well known that base molecules can adsorb CO_2 molecules, e.g., amines are used in commercial scrubbers to remove CO_2 from gas streams. In this study, 2-methylimidazole in the ZIF-8 structure was converted to porous carbon functionalized with N-species during pyrolysis. Those N-species doped in the porous carbon reveal basic properties of the synthesized materials, while the metal clusters (zinc) were partially removed from the material during the pyrolysis process. Consequently, the acid sites (zinc) and the basic sites present in the catalytic material take part in the catalytic reaction for the CO_2 cycloaddition reaction.

Based on the obtained experimental results and previously published reports, a plausible reaction mechanism was proposed for the CO_2 cycloaddition over metal embedded N-doped porous carbon catalysts (Figure 8). The reaction mechanism for the CO_2 cycloaddition can be attributed to the presence of the Lewis acid sites originating from metal species (Zn or Co) activating the epoxide substrate (ring-opening). Meanwhile, the lone pair electrons of the nitrogen act as a base, interacting with the electron-deficient carbon in CO_2 [45]. Nitrogen species could act as electron donors in carbon material, causing a shift in the Fermi level to the valence bands [46]. Next, a nucleophilic attack of N-species occurs on the carbon atom of CO_2 . The oxygen of the activated carbon dioxide binds with the carbon of the opened epoxide, forming an intermediate species. Finally, the cyclic carbonate molecule is formed via a nucleophilic attack of the oxygen from the opened epoxide during which the weak N–C dative bond will be disrupted, resulting in the product's easy desorption due to the nitrogen's conjugated nature in the carbon matrix, and the vacated sites for the following reaction cycle are generated. Moreover, the catalytic activity for the CO_2 cycloaddition into epoxides strongly depends on the type and relative abundance of the surface functional groups (here, pyrrolic N) [31,47,48]. The pyrrolic N is the most active site compared with the other N species for the CO_2 fixation reaction [22].

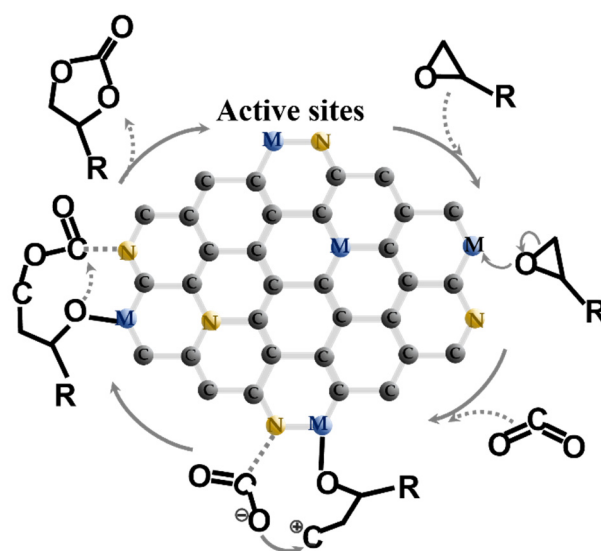


Figure 8. Proposed catalytic mechanism for the cycloaddition of epoxides and CO_2 into cyclic carbonates catalyzed by N-doped porous carbon (M: Acid sites derived from metallic zinc or cobalt, N: Basic sites of N-doped carbon derived from 2-MIM decomposition during pyrolysis).

3. Materials and Methods

3.1. Materials and Synthesis

All chemical reagents for synthesis materials and catalytic reaction were purchased from Aladdin chemical and used as received without further purification. To prepare

N-doped porous carbonaceous materials, ZIFs (ZIF-8, ZnCo-ZIF, and ZIF-67) were firstly synthesized before using them as template material for the pyrolysis process (Figure 9). The ZIFs were synthesized via a green method using water as a solvent at room temperature with a slightly modified synthesis procedure from the previous report [23]. A typical synthesis of ZIF-8 and ZIF-67, 10 mmol of metal source ($\text{Zn}(\text{NO}_3)_2 \cdot 6\text{H}_2\text{O}$ or $\text{Co}(\text{NO}_3)_2 \cdot 6\text{H}_2\text{O}$) and 80 mmol of ligand source (2-methylimidazole, Hmim) were separately dissolved in 100 mL of deionized water. For the bimetallic ZIF, a 50:50 ratio of $\text{Zn}(\text{NO}_3)_2 \cdot 6\text{H}_2\text{O}$ and $\text{Co}(\text{NO}_3)_2 \cdot 6\text{H}_2\text{O}$ with a constant total molar ratio (10 mmol) was applied for the ZnCo-ZIF synthesis. Triethylamine (5 mL) as a deprotonating agent was added to an aqueous Hmim solution before adding to the aqueous metal solution. The mixture was vigorously stirred at room temperature for 24 h, and then the precipitated solid was separated using a centrifuge (9500 rpm, 5 min). The obtained solids were washed with deionized water three times or until the obtained solution after centrifugal was clear. The solid products were dried at 100 °C under vacuum overnight before further use or analysis. After that, the ZIFs templates were pyrolyzed to synthesize carbonaceous materials at 1000 °C in a quartz tube furnace using a heating rate of 10 °C/min under 5% H_2 in Ar (50 cm^3/min) for 1 h. After cooling to room temperature, the products were collected and stored in a desiccator to prevent moisture sorption. The obtained carbonaceous products were labeled as Zn/CN, ZnCo/CN, and Co/CN, deriving from template material of ZIF-8, ZnCo-ZIF, and ZIF-67, respectively. Furthermore, more details of synthesis materials are provided in the supporting information.

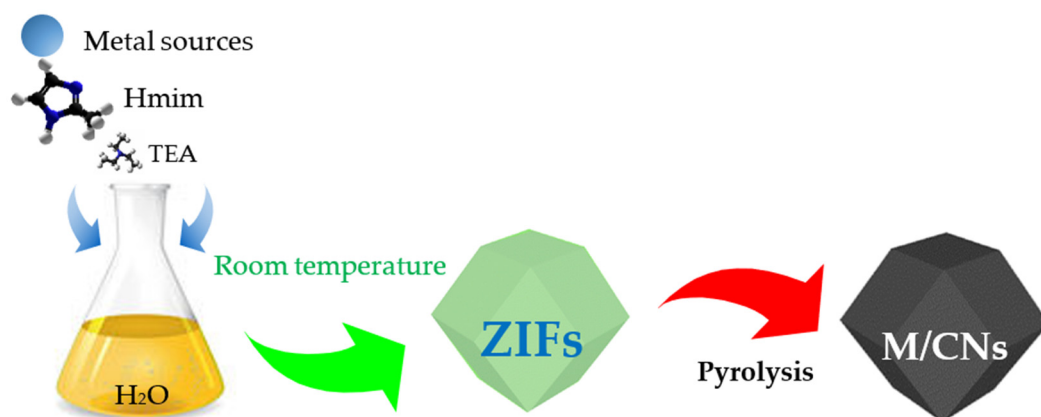


Figure 9. Schematic presentation of the synthesis procedure of N-doped porous carbonaceous materials deriving from zeolitic imidazole frameworks.

3.2. Material Characterization

The crystal structure of synthesized materials was analyzed by powder X-ray diffraction (Bruker D8 Advance diffractometer, Bragg-Brentano geometry, $\text{Cu K}\alpha$ radiation). The data were typically collected in the 2θ range of 10–80°, scanning step 0.02°, and 0.2 s per step. Scanning electron microscope (FE-SEM, Zeiss Ultra Plus) and transmission electron microscopy (TEM, JEM-2100F) with energy-dispersive X-ray spectroscopy (EDS), operating at a high voltage of 200 kV, were carried out to investigate the morphology of the materials. The surface area and adsorption-desorption isotherm measurements were performed using a Micromeritics instrument (ASAP 2020) at 77 K using liquid nitrogen as a coolant. Before the adsorption measurements, the samples (50–100 mg) were evacuated at 180 °C under a dynamic vacuum for about 3 h. The micropore surfaces were calculated by the Brunauer–Emmett–Teller (BET) and Langmuir method ($0.005 < P/P_0 < 0.05$). The Horvath–Kawazoe method was applied for micropore analysis. X-ray photoelectron spectroscopy (XPS) measurements were conducted on a Kratos Axis Ultra DLD (delay-line detector) spectrometer equipped with a monochromatic $\text{Al K}\alpha$ X-ray source (1486.6 eV). All binding energies were referenced to the C1s peak at 284.9 eV of the surface adventitious carbon. The CasaXPS Processing software was applied to deconvolute the results. Thermogravimetric

analyses were carried out on a Netzsch (STA449c/3/G) instrument using a heating rate of $10\text{ }^{\circ}\text{C min}^{-1}$ under a nitrogen atmosphere. Fourier transformed infrared spectra (FT-IR) were recorded on a Nicolet 6700 FT-IR spectrometer with KBr pellets in the wave range of $4000\text{ to }400\text{ cm}^{-1}$. The metals content was determined via inductively coupled plasma optical emission spectrometry (ICP-OES, Prodigy 7). The carbon and nitrogen elements were analyzed by CHN element analysis (Vario EL cube). The basic properties of the materials were examined via temperature-programmed desorption (TPD) (AutoChem II 2920) using NH_3 as the probe gases. The sample was first pre-treated at $150\text{ }^{\circ}\text{C}$ under He flow for 3 h before TPD analysis. (Details are available in the Supplementary Materials).

3.3. Cycloaddition Reaction

For the catalytic reactions, 9.2 mmol of epoxide and 50 mg of catalyst were charged in a reactor (high-pressure glass bottle, 15 mL) for the low-pressure experiment, and in a stainless steel high-pressure reactor (15 mL, XINGDA Company, Beijing, China) for the high-pressure experiments. Subsequently, the reactor was purged for a few seconds before pressuring with CO_2 (99.9%) via a pressure regulator and keeping a constant pressure along with the reaction time. The reactor was immersed in a pre-heat oil bath with a thermocouple (IKA RCT basic) under a setting reaction temperature and time. After that, the reactor was cooled to room temperature, and the excess gas was vented out. The 1,3,5-trimethylbenzene, as the internal standard (3 mmol), and CDCl_3 (1 mL) were added to the reaction mixture. The final product was analyzed by nuclear magnetic resonance (Bruker NMR 500 MHz: ^1H and ^{13}C). For a recycling experiment, the catalyst was separated from the reaction mixture via centrifugal and washed several times with methanol before drying under vacuum at $90\text{ }^{\circ}\text{C}$ for 6 h before the subsequent use (Details are available in the Supplementary Materials).

4. Conclusions

Hierarchical porous N-doped carbon materials derived from zeolitic imidazolate frameworks as template materials were synthesized and characterized. Metal embedded in N-doped porous carbon materials was obtained via tuning structural ZIF templates (pyrolysis). The metallic dispersion (Zn, Co) with the N-species (pyrrolic-, pyridinic-, and ammonium-N) in hierarchically porous carbon demonstrated to be the key active sites over the embedded metal species to catalyze the cycloaddition of CO_2 with epoxides into cyclic carbonates. The pyrrolic N becomes dominant over pyridinic and ammonium N-species in Zn/CN at a higher pyrolysis temperature, demonstrating the importance of catalytic sites for the metal-and N-doped porous carbon catalysts. The lack of N-species in commercial carbon, metal sources, etc., resulted in no reaction products, confirming the significance of N-species for the catalytic reaction. Moreover, the metal de-coordination and partial elimination from the template framework provided different N-species, as well as metallic species and hierarchical pore structures that enhanced access to the inner active sites. The synthesized catalyst exhibited a high catalytic performance combined with thermal and chemical stability, as demonstrated by the recycling experiments (>7 cycles). Furthermore, the optimized reaction conditions, near ambient pressure, can be applied without solvent and co-catalyst, providing a green procedure based on a heterogeneous catalyst to produce cyclic carbonates by the synergistic activation of CO_2 and epoxide substrates. Therefore, two novelties can be highlighted. Firstly, in the catalyst synthesis, the template ZIFs were synthesized under room temperature and organic solvent-free (aqua-solution). A facile method was processed via the thermal treatment of template ZIFs to derive metal de-coordination and encapsulation in N-doped carbon. Secondly, the synthesized materials were directly used as catalysts without post-treatment or additional functional requirements in the catalytic reaction. The catalysts showed good performance under mild conditions at $80\text{--}90\text{ }^{\circ}\text{C}$ and atmospheric (1 bar of CO_2 pressure) without solvent and co-catalyst. The catalyst characterization reveals well-dispersed active sites in a hierarchical porous (micro and mesoporous) material. The catalysts' high surface area promotes the mass transfer to

access the active species and substrates. The “green” catalyst is a robust heterogeneous catalyst that maintains excellent performance for multiple runs.

Supplementary Materials: The following supporting information can be downloaded at: <https://www.mdpi.com/article/10.3390/catal12040427/s1>. Figure S1. The muffle furnace: TL 1200, Nanjing Bo Yun Tong Instrument Technology Co., Ltd.; Figure S2. Crystal morphologies of as synthesized ZIF-8 (a), ZIF-67 (b), and bimetal ZnCo-ZIF (c) using SEM; Figure S3. N₂ adsorption isotherms at 77K of template ZIF-8, ZIF-67, and bimetal ZnCo-ZIF; Figure S4. TGA analyses of ZIF series from room temperature up to 800 °C with a heating rate of 10 °C/min under Ar atmosphere (20 cc/min). All the ZIF-8 samples were activated at 200 °C under vacuum for 3 h before TGA analysis; Figure S5. Transmission electron microscope (TEM) image and elemental mapping (EDX) of ZIF-8. High-resolution transmission electron microscope (HR-TEM) and energy dispersive X-ray spectroscopy (EDS) analyses were carried out using a JEOL JEM-2100F microscope operating at a high voltage of 200 kV; Figure S6. N₂ adsorption isotherm at 77 K and pore size distribution (BJH) of Zn/CN-1000 (a,b), ZnCo/CN-1000 (c,d), and bimetal Zn/CN-1000 (e,f); Figure S7. FTIR spectra of pyrolyzed ZIF compared with organic linker; Figure S8. High-resolution XPS spectra of zinc (a) and cobalt region (b) from Zn/CN, Co/CN and ZnCo/CN; Figure S9. CO₂-TPD analysis of synthesized porous carbon: ZnCo/CN (bottom), Zn/CN(middle), and Co/CN(top); Figure S10. Nitrogen adsorption isotherm at 77K (a) and CO₂ adsorption at 273K (b) on Carbon graphite; Figure S11. (a) N₂ adsorption isotherm at 77K of Zn/CN after reaction (spend catalyst). (b) XRD diffraction of fresh and spend Zn/CN; Figure S12. ¹H-NMR (a) and ¹³C-NMR (b) spectrum in CDCl₃ of the product [3-chloro-1-propene carbonate] obtained from the conversion of epichlorohydrin with CO₂. Reaction condition: 850 mg epichlorohydrin, 50 mg of Zn/Cn-1000, 140 °C, 8 bar of CO₂, 8 h; Figure S13. The NMR of the recycling experiment using Zn/CN-1000 (reaction conditions: epichlorohydrin 850 mg (9.2 mmol), Catalyst 50 mg, 90 °C, 1.5 bar of CO₂ pressure for 24 h); Figure S14. ¹H NMR spectrum in CDCl₃ of the product [4-(bromomethyl)-1,3-dioxolan-2-one] obtained from the conversion of epibromohydrin using Zn/CN-1000 (50 mg), CO₂ pressure 1.5 bar, 80 °C for 24 h; Figure S15. ¹H-NMR (a) and ¹³C-NMR (b) spectrum in CDCl₃ of the product [4-butoxymethyl]-1,3-dioxolan-2-one] obtained from the reaction mixture of butyl glycidyl ether using Zn/CN-1000 (50 mg), CO₂ pressure 8 bar, 140 °C for 24 h; Figure S16. ¹H-NMR (a) and ¹³C-NMR (b) spectrum in CDCl₃ of the product [4-butyl-1,3-dioxolan-2-one] obtained from the reaction mixture of 1,2-epoxyhexane using Zn/CN-1000 (50 mg), CO₂ pressure 8 bar, 140 °C for 24 h; Figure S17. ¹H-NMR (a) and ¹³C-NMR (b) spectrum in CDCl₃ of the product [Allyloxymethyl-1,3-dioxlan-2-one] obtained from the reaction mixture of allyl glycidyl ether using Zn/CN-1000 (50 mg), CO₂ pressure 8 bar, 140 °C for 24 h; Figure S18. ¹H-NMR spectrum in CDCl₃ of the product [4-Methyl-1,3-dioxlan-2-one] obtained from the reaction mixture of propylene oxide using Zn/CN-1000 (50 mg), CO₂ pressure 1.5 bar, 80 °C for 24 h. Table S1. The mole and mass/volume of reagent were obtained to synthesis ZIF-8, ZIF-67 and dual metal Zn/Co-ZIF; Table S2. The elemental composition of materials; Table S3. Overview of catalytic performance under different reaction conditions; Table S4. Summary catalyst performance and reaction system based on the carbon-based materials for the synthesis of cyclic carbonates with reaction condition.

Author Contributions: Methodology, investigation, data curation by C.Q. and M.L.; writing—original draft by J.W.; conceptualization, methodology, investigation, writing—original draft by S.C.; writing—review by S.Z.; conceptualization, resources, supervision, writing—review and editing by F.V. All authors have read and agreed to the published version of the manuscript.

Funding: This research received no external funding.

Acknowledgments: The authors are grateful to the State Key Lab of Advanced Technology for Materials Synthesis and Processing for financial support (Wuhan University of Technology). S.C. acknowledges the support of the National Natural Science Foundation of China (No. 21950410754).

Conflicts of Interest: The authors declare no conflict of interest.

References

1. Georgakilas, V.; Perman, J.A.; Tucek, J.; Zboril, R. Broad family of carbon nanoallotropes: Classification, chemistry, and applications of fullerenes, carbon dots, nanotubes, graphene, nanodiamonds, and combined superstructures. *Chem. Rev.* **2015**, *115*, 4744–4822. [[CrossRef](#)] [[PubMed](#)]
2. Su, D.S.; Perathoner, S.; Centi, G. Nanocarbons for the development of advanced catalysts. *Chem. Rev.* **2013**, *113*, 5782–5816. [[CrossRef](#)]
3. Kumar, S.; Kumar, P.; Deb, A.; Maiti, D.; Jain, S.L. Graphene oxide grafted with iridium complex as a superior heterogeneous catalyst for chemical fixation of carbon dioxide to dimethylformamide. *Carbon* **2016**, *100*, 632–640. [[CrossRef](#)]
4. Liang, C.; Li, Z.; Dai, S. Mesoporous carbon materials: Synthesis and modification. *Angew. Chem. Int. Ed.* **2008**, *47*, 3696–3717. [[CrossRef](#)] [[PubMed](#)]
5. Lee, J.; Kim, J.; Hyeon, T. Recent progress in the synthesis of porous carbon materials. *Adv. Mater.* **2006**, *18*, 2073–2094. [[CrossRef](#)]
6. Yang, R.T.; Wang, Y. Catalyzed hydrogen spillover for hydrogen storage. *J. Am. Chem. Soc.* **2009**, *131*, 4224–4226. [[CrossRef](#)] [[PubMed](#)]
7. Hu, B.; Wang, K.; Wu, L.; Yu, S.; Antonietti, M.; Titirici, M. Engineering carbon materials from the hydrothermal carbonization process of biomass. *Adv. Mater.* **2010**, *22*, 813–828. [[CrossRef](#)]
8. Kyotani, T. Control of pore structure in carbon. *Carbon* **2000**, *38*, 269–286. [[CrossRef](#)]
9. Flandrois, S.; Simon, B. Carbon materials for lithium-ion rechargeable batteries. *Carbon* **1999**, *37*, 165–180. [[CrossRef](#)]
10. Joo, S.H.; Choi, S.J.; Oh, I.; Kwak, J.; Liu, Z.; Terasaki, O.; Ryoo, R. Ordered nanoporous arrays of carbon supporting high dispersions of platinum nanoparticles. *Nature* **2001**, *412*, 169–172. [[CrossRef](#)]
11. Jordá-Beneyto, M.; Suárez-García, F.; Lozano-Castello, D.; Cazorla-Amorós, D.; Linares-Solano, A. Hydrogen storage on chemically activated carbons and carbon nanomaterials at high pressures. *Carbon* **2007**, *45*, 293–303. [[CrossRef](#)]
12. Juárez-Pérez, E.J.; Calvo, E.G.; Arenillas, A.; Menéndez, J.A. Precise determination of the point of sol–gel transition in carbon gel synthesis using a microwave heating method. *Carbon* **2010**, *48*, 3305–3308. [[CrossRef](#)]
13. Vitillo, J.G.; Crocellà, V.; Bonino, F. ZIF-8 as a Catalyst in ethylene oxide and propylene oxide reaction with CO₂ to cyclic organic carbonates. *ChemEngineering* **2019**, *3*, 60. [[CrossRef](#)]
14. Kuruppathparambil, R.R.; Babu, R.; Jeong, H.M.; Hwang, G.Y.; Jeong, G.S.; Kim, M.; Kim, D.W.; Park, D.W. A solid solution zeolitic imidazolate framework as a room temperature efficient catalyst for the chemical fixation of CO₂. *Green Chem.* **2016**, *18*, 6349–6356. [[CrossRef](#)]
15. Xiang, W.L.; Shen, C.Y.; Lu, Z.; Chen, S.; Li, X.; Zou, R.; Zhang, Y.P.; Liu, C.J. CO₂ cycloaddition over ionic liquid immobilized hybrid zeolitic imidazolate frameworks: Effect of Lewis acid/base sites. *Chem. Eng. Sci.* **2021**, *233*, 116429. [[CrossRef](#)]
16. Xia, W.; Mahmood, A.; Zou, R.; Xu, Q. Metal–organic frameworks and their derived nanostructures for electrochemical energy storage and conversion. *Energy Environ. Sci.* **2015**, *8*, 1837–1866. [[CrossRef](#)]
17. Zhao, Y.; Song, Z.X.; Li, X.; Sun, Q.; Cheng, N.; Lawes, S.; Sun, X.L. Metal organic frameworks for energy storage and conversion. *Energy Storage Mater.* **2016**, *2*, 35–62. [[CrossRef](#)]
18. Zhong, W.; Liu, H.; Bai, C.; Liao, S.; Li, Y. Base-free oxidation of alcohols to esters at room temperature and atmospheric conditions using nanoscale co-based catalysts. *ACS Catal.* **2015**, *5*, 1850–1856. [[CrossRef](#)]
19. Chen, C.; Wang, Z.Q.; Gong, Y.Y.; Wang, J.C.; Yuan, Y.; Cheng, H.; Sang, W.; Chaemchuen, S.; Verpoort, F. Cobalt embedded in nitrogen-doped porous carbon as a robust heterogeneous catalyst for the atom-economic alcohol dehydrogenation to carboxylic acids. *Carbon* **2021**, *174*, 284–294. [[CrossRef](#)]
20. Santos, V.P.; Wezendonk, T.A.; Jaén, J.J.D.; Dugulan, A.I.; Nasalevich, M.A.; Islam, H.-U.; Chojecki, A.; Sartipi, S.; Sun, X.; Hakeem, A.A.; et al. Metal organic framework-mediated synthesis of highly active and stable Fischer-Tropsch catalysts. *Nat. Commun.* **2015**, *6*, 6451. [[CrossRef](#)]
21. Sun, X.; Olivos-Suarez, A.I.; Oar-Arteta, L.; Rozhko, E.; Osadchii, D.; Bavykina, A.; Kapteijn, F.; Gascon, J. Metal-organic-framework mediated cobalt/N-doped carbon hybrids as efficient and chemoselective catalysts for the hydrogenation of nitroarenes. *ChemCatChem* **2017**, *9*, 1854. [[CrossRef](#)]
22. Chaemchuen, S.; Xiao, X.; Ghadamyari, M.; Mousavi, B.; Klomkliang, N.; Yuan, Y.; Verpoort, F. Robust and efficient catalyst derived from bimetallic Zn/Co zeolitic imidazolate frameworks for CO₂ conversion. *J. Catal.* **2019**, *370*, 38–45. [[CrossRef](#)]
23. Khan, I.U.; Othman, M.H.D.; Ismail, A.F.; Ismail, N.; Jaafar, J.; Hashim, H.; Rahman, M.A.; Jilani, A. Structural transition from two-dimensional ZIF-L to three-dimensional ZIF-8 nanoparticles in aqueous room temperature synthesis with improved CO₂ adsorption. *Mater. Charact.* **2018**, *136*, 407–416. [[CrossRef](#)]
24. Zhou, K.; Mousavi, B.; Luo, Z.; Phatanasri, S.; Chaemchuen, S.; Verpoort, F. Characterization and properties of Zn/Co zeolitic imidazolate frameworks vs. ZIF-8 and ZIF-67. *J. Mater. Chem.* **2017**, *5*, 952–957. [[CrossRef](#)]
25. Kaneti, Y.V.; Tang, J.; Salunkhe, R.R.; Jiang, X.; Yu, A.; Wu, K.C.W.; Yamauchi, Y. Nanoarchitected design of porous materials and nanocomposites from metal-organic frameworks. *Adv. Mater.* **2017**, *29*, 1604898. [[CrossRef](#)]
26. Liu, B.; Shioyama, H.; Akita, T.; Xu, Q. Metal-organic framework as a template for porous carbon synthesis. *J. Am. Chem. Soc.* **2008**, *130*, 5390–5391. [[CrossRef](#)]
27. Meng, J.S.; Niu, C.J.; Xu, L.H.; Li, J.T.; Liu, X.; Wang, X.P.; Wu, Y.Z.; Xu, X.M.; Chen, W.Y.; Li, Q.; et al. General oriented formation of carbon nanotubes from metal-organic frameworks. *J. Am. Chem. Soc.* **2017**, *139*, 8212–8221. [[CrossRef](#)]

28. Xia, B.Y.; Yan, Y.; Li, N.; Wu, H.B.; Lou, X.W.; Wang, X. A metal-organic framework-derived bifunctional oxygen electrocatalyst. *Nat. Energy* **2016**, *1*, 15006. [[CrossRef](#)]
29. Hayashi, M. Oxidation using activated carbon and molecular oxygen system. *Chem. Rec.* **2008**, *8*, 252–267. [[CrossRef](#)]
30. Konwar, L.J.; Sugano, Y.; Chutia, R.S.; Shchukarev, A.; Mäki-Arvela, P.; Kataki, R.; Mikkola, J.-P. Sustainable synthesis of N and P co-doped porous amorphous carbon using oil seed processing wastes. *Mater. Lett.* **2016**, *173*, 145–148. [[CrossRef](#)]
31. Fan, X.Q.; Zhang, L.X.; Zhang, G.B.; Shu, Z.; Shi, J.L. Chitosan derived nitrogen-doped microporous carbons for high performance CO₂ capture. *Carbon* **2013**, *61*, 423–430. [[CrossRef](#)]
32. Sevilla, M.; Valle-Vigón, P.; Fuertes, A.B. N-doped polypyrrole-based porous carbons for CO₂ capture. *Adv. Funct. Mater.* **2011**, *21*, 2781–2787. [[CrossRef](#)]
33. Yang, Q.; Yang, C.-C.; Lin, C.-H.; Jiang, H.-L. Metal-organic-framework-derived hollow n-doped porous carbon with ultrahigh concentrations of single zn atoms for efficient carbon dioxide conversion. *Angew. Chem. Int. Ed.* **2019**, *58*, 3511–3515. [[CrossRef](#)] [[PubMed](#)]
34. Wang, T.T.; Kou, Z.K.; Mu, S.C.; Liu, J.P.; He, D.P.; Amiin, I.S.; Meng, W.; Zhou, K.; Luo, Z.X.; Chaemchuen, S.; et al. 2D Dual-metal zeolitic-imidazolate-framework-(ZIF)-derived bifunctional air electrodes with ultrahigh electrochemical properties for rechargeable zinc-air batteries. *Adv. Funct. Mater.* **2018**, *28*, 1705048. [[CrossRef](#)]
35. Wang, N.Y.; Huang, X.H.; Zhang, L.; Hu, J.S.; Chao, Y.M.; Zhao, R.K. Pyrolysis transformation of ZIF-8 wrapped with polytriazine to nitrogen enriched core-shell polyhedrons carbon for supercapacitor. *Front. Chem. Sci. Eng.* **2021**, *15*, 944–953. [[CrossRef](#)]
36. Kim, M.; Park, T.; Wang, C.; Tang, J.; Lim, H.; Hossain, M.S.A.; Konarova, M.; Yi, J.W.; Na, J.; Kim, J.; et al. Tailored nanoarchitecturing of microporous ZIF-8 to hierarchically porous double-shell carbons and their intrinsic electrochemical property. *ACS Appl. Mater. Interfaces* **2020**, *12*, 34065–34073. [[CrossRef](#)]
37. Banks, C.E.; Crossley, A.; Salter, C.; Wilkins, S.J.; Compton, R.G. Carbon nanotubes contain metal impurities which are responsible for the “electrocatalysis” seen at some nanotube-modified electrodes. *Angew. Chem. Int. Ed.* **2006**, *45*, 2533–2537. [[CrossRef](#)]
38. Mousavi, B.; Chaemchuen, S.; Ezugwu, C.I.; Yuan, Y.; Verpoort, F. The effect of synthesis procedure on the catalytic performance of isostructural ZIF-8. *Appl. Organomet. Chem.* **2017**, *32*, e4062. [[CrossRef](#)]
39. Ciprian, M.; Ruiz, K.H.; Kassymova, M.; Wang, T.; Zhuiykov, S.; Chaemchuen, S.; Tu, R.; Verpoort, F. 3D derived N-doped carbon matrix from 2D ZIF-L as an enhanced stable catalyst for chemical fixation. *Microporous Mesoporous Mater.* **2019**, *285*, 80–88. [[CrossRef](#)]
40. Herskovitz, T. Organic and Bio-organic chemistry of carbon dioxide. *Organometallics* **1983**, *2*, 201–202. [[CrossRef](#)]
41. Abila, M.; Choi, J.C.; Sakakura, T. Halogen-free process for the conversion of carbon dioxide to urethanes by homogeneous catalysis. *Chem. Commun.* **2001**, 2238–2239. [[CrossRef](#)] [[PubMed](#)]
42. Samikannu, A.; Konwar, L.J.; Mäki-Arvela, P.; Mikkola, J.P. Renewable N-doped active carbons as efficient catalysts for direct synthesis of cyclic carbonates from epoxides and CO₂. *Appl. Catal. B Environ.* **2019**, *241*, 41–51. [[CrossRef](#)]
43. Guo, Y.C.; Feng, L.; Wu, C.C.; Wang, X.M.; Zhang, X. Confined pyrolysis transformation of ZIF-8 to hierarchically ordered porous Zn-N-C nanoreactor for efficient CO₂ photoconversion under mild conditions. *J. Catal.* **2020**, *390*, 213–223. [[CrossRef](#)]
44. Chizallet, C.; Lazare, S.; Bazer-Bachi, D.; Bonnier, F.; Lecocq, V.; Soyer, E.; Quoineaud, A.-A.; Bats, N. Catalysis of transesterification by a nonfunctionalized metal-organic framework: Acido-basicity at the external surface of ZIF-8 probed by FTIR and ab initio calculations. *J. Am. Chem. Soc.* **2010**, *132*, 12365–12377. [[CrossRef](#)] [[PubMed](#)]
45. Leal, O.; Bolívar, C.; Ovalles, C.; García, J.J.; Espidel, Y. Reversible adsorption of carbon dioxide on amine surface-bonded silica gel. *Inorg. Chim. Acta* **1995**, *240*, 183–189. [[CrossRef](#)]
46. Cruz-Silva, E.; Cullen, D.A.; Gu, L.; Romo-Herrera, J.M.; Muñoz-Sandoval, E.; López-Urías, F.; Sumpter, B.G.; Meunier, V.; Charlier, J.C.; Smith, D.J.; et al. Heterodoped nanotubes: Theory, synthesis, and characterization of phosphorus–nitrogen doped multiwalled carbon nanotubes. *ACS Nano* **2008**, *2*, 441–448. [[CrossRef](#)] [[PubMed](#)]
47. Li, Y.; Zou, B.; Hu, C.; Cao, M. Nitrogen-doped porous carbon nanofiber webs for efficient CO₂ capture and conversion. *Carbon* **2016**, *99*, 79–89. [[CrossRef](#)]
48. Ma, X.Y.; Zou, B.; Cao, M.H.; Chen, S.L.; Hu, C.W. Nitrogen-doped porous carbon monolith as a highly efficient catalyst for CO₂ conversion. *J. Mater. Chem. A* **2014**, *2*, 18360–18366. [[CrossRef](#)]